Density-Functional Calculations on Platinum Nanoclusters: Pt_{13}, Pt_{38}, and Pt_{55}

Edoardo Aprà[†] and Alessandro Fortunelli*[,‡]

Theory, Modeling & Simulation, Environmental Molecular Sciences Laboratory, Pacific Northwest National Laboratory, P.O. Box 999, Richmond, Washington 99352, and Molecular Modeling Laboratory, Istituto per i Processi Chimico-Fisici (IPCF) del C.N.R., via V. Alfieri 1, 56010, Ghezzano (PI), Italy

Received: November 28, 2002; In Final Form: February 20, 2003

The results of an accurate density-functional study of the structure, energetics and electronic structure of Pt_n clusters (with $n = 13$, 38, and 55) are presented. For Pt_{38}, a truncated octahedral geometry is considered; for Pt_{13} and Pt_{55}, icosahedral, truncated decahedral, and cuboctahedral geometries are considered. In each case, the structure of the neutral and positively and negatively charged clusters is fully optimized within the given symmetry group. For Pt_{13}, allowing symmetry breaking starting from the symmetrical structures derives additional local minima. The computational procedure is thoroughly tested to keep numerical accuracy under control. From the electronic structure point of view, it is found that these systems start developing metallic characteristics, with ionization introducing small changes. From the structural point of view, for Pt_{13} the icosahedral configuration is not favored, whereas it becomes the ground state for Pt_{55}, in agreement with the predictions of atom−atom potentials. Moreover, the lowest energy configuration of Pt_{13} is a symmetry-broken D_{4h} one, while for Pt_{38} and Pt_{55} a peculiar rearrangement is found, corresponding to an expansion (reconstruction) of the atoms lying on (111) or (100) faces.

1. Introduction

The chemistry and physics of metal clusters have attracted much attention in recent years (see, for example, ref 1) for their peculiar structural, electronic, optical, etc., properties. The wealth of experimental data has prompted an intense theoretical effort devoted to elucidate the mechanisms at work in this class of systems. The theoretical literature on isolated metal clusters has dealt with both the structural and the electronic properties.[2−16] From the structural point of view, attention has usually concentrated on high-symmetry configurations. Structures corresponding to pieces of the bulk crystals (fcc, bcc, etc.), which should be the lowest energy ones for very large aggregates, have been compared with others containing C_5 axes (icosahedral or decahedral) which are incompatible with translational symmetry but are expected to be good competitors for smaller clusters, due to more favorable surface energies at the expense of introducing internal strain.[2−9,13] One thus expects a crossover among these structures with increasing size, with the icosahedral configurations dominating at small sizes, the decahedral configurations dominating at intermediate sizes, and the crystalline configurations eventually dominating at large sizes (see, for example, ref 7). More recently, "amorphous" arrangements have also been proposed as possible lowest energy structures for small clusters.[11,12,15] From the electronic point of view, the limitations of simplified approached such as the "jellium" model have been pointed out,[13] and various techniques have been proposed to analyze the shell structure of the one-electron energy levels[10] and to study the behavior of the cluster properties with size (and extrapolate them to the bulk limit).[8,9,13,14]

In this context, platinum clusters undoubtedly represent a class of systems of great importance because of the role they play in many catalytic processes (they are considered one of the most important materials in heterogeneous catalysis[1]). A theoretical understanding of their structural and electronic properties is essential to the first-principle prediction of their behavior. Moreover, platinum is especially interesting also from a purely theoretical point of view because the crossover between icosahedral, decahedral and crystalline structures is expected to occur at small size.[7] Despite this, in the literature one cannot find many calculations on Pt_n clusters with $n \geq 13$,[10−12,14] probably due to the fact that platinum (as a third-row transition metal) simultaneously presents all the difficulties connected with s/p-d mixing and relativistic effects.

Experimentally, the structure of Pt_n clusters with $n \leq 200$ is still unclear: for clusters with diameter >10 nm[17] or even ∼2 nm[18] crystalline geometries seem to be preferred, but other structural forms might be favorite for smaller aggregates.[19]

In the present article, density-functional (DF) calculations on Pt_{13}, Pt_{38}, and Pt_{55} neutral clusters and their singly charged ions will be presented. Highly symmetrical structures have been considered: truncated octahedron (O_h symmetry group) for Pt_{38}, cuboctahedron (O_h), truncated decahedron (D_{5h}), and icosahedron (I_h) for Pt_{13} and Pt_{55} (see Figure 1 for schematic pictures). All the structures have been fully optimized within the corresponding symmetry group. In the case of Pt_{13}, symmetry breaking starting from the symmetrical structures has been allowed, producing configurations corresponding to additional local minima. The chosen symmetrical structures are the most likely ordered candidates as the lowest energy ones for finite systems.[2,3] Moreover, from their comparison it is possible to predict the general crossover behavior among the different structural motifs (see, for example, ref 7 and references therein). Investigation on "amorphous" structures[11,12,15] is deferred to future work.

* Address for correspondence. IPCF-CNR, v. V. Alfieri 1, 56010, Ghezzano (PI), Italy. E-mail: fortunelli@icqem.pi.cnr.it. Phone: + 39-050-3152447. Fax: + 39-050-3152442.

[†] Pacific Northwest National Laboratory.

[‡] Molecular Modeling Laboratory IPCF-CNR.

10.1021/jp0275793 CCC: $25.00
Published on Web 04/01/2003

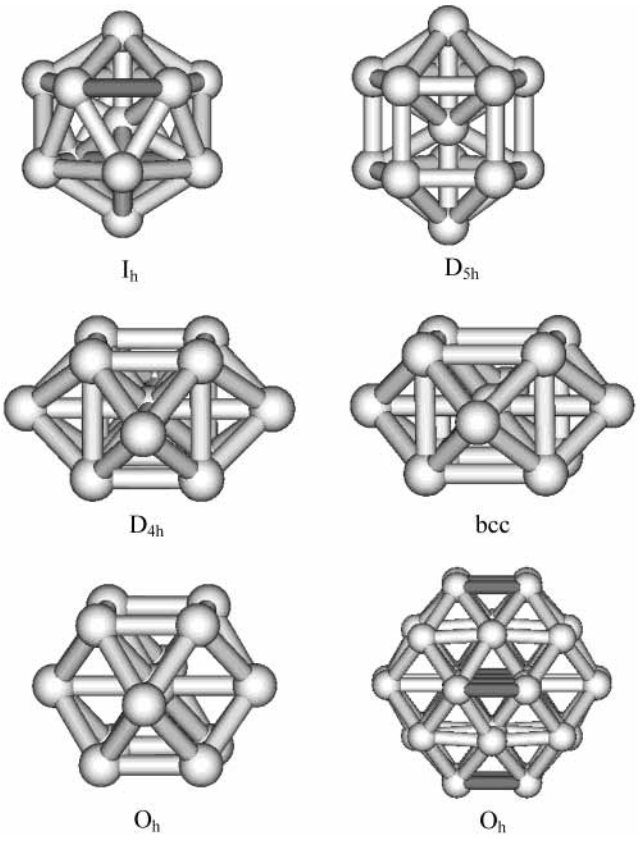

Figure 1. Schematic drawings of the Pt_{13} and Pt_{38} structures considered in the text.

From a computational point of view, symmetry is fully exploited to reduce the computational effort, so as to make a computationally accurate approach feasible on these large and complicated systems. This should also provide a standard against which more approximate approaches (many-body atom−atom potentials,[7,20] tight-binding methods,[21,22] etc.) can be contrasted and parametrized. Preliminary DF calculations on Pt_{13} and Pt_{55} cuboctahedral clusters have been previously presented.[14]

In section 2, the computational approach and the theoretical method will be detailed. In section 3, the results of the DF calculations will be presented and discussed. The main conclusions will be summarized in section 4.

2. Computational Details and Method

All the calculations were carried out with the DF module of the NWChem computational chemistry package (release 4.1)[23] that uses Gaussian-type orbitals (GTOs) for the solution of the Kohn−Sham equations.

An effective core potential (ECP)[24] was used to represent the nucleus plus inner-shell (up to the 4f shell) core electrons interactions with all valence electrons; thus only the outer-core (5s and 5p shells) plus valence electron wave function is solved for explicitly. This ECP incorporates spin−orbit-averaged relativistic effects. Two atomic orbital bases were used for describing the outer-core plus valence electrons, both derived from a (7s6p5d)/[6s3p2d] basis set.[25] In the first one (basis set A), the s-functions were left uncontracted, the first p- and d-contractions of 4 GTOs were split into three and one GTOs, corresponding to a (7s6p5d)/[7s4p3d] basis set. In the second one (basis set B), we removed the most diffuse p-function that causes numerical instabilities in these highly condensed systems, and split the first p-contraction as above, to get a (7s5p5d)/[6s3p2d] basis set.

All the calculations were performed spin-unrestricted, using the Becke functional[26] for exchange and the Perdew−Wang functional[27] for correlation, hereafter referred to with the acronym BPW91. The BPW91 functional has been selected as the gradient-corrected one which gives optimal values for the $5d^96s^1 \rightarrow 5d^{10}$ excitation energy of the Pt atom and dissociation energy of the Pt_2 molecule[28] (hybrid functionals should not be used for metal clusters[14]). We refer to refs 8−11, 14, and 16 for a discussion of the DF approach as applied to transition metal clusters.

In addition to the basis set for the Kohn−Sham orbitals, a charge density fitting basis was used to compute the Coulomb potential according to the method described in refs 29 and 30. The (9s3p3d2f2g) basis set used was derived from the one described in ref 31. Numerical tests on Pt_{13}, Pt_{38}, and Pt_{55} have shown that the effect of this approximation on the total energy differences among the various configurations is of the order of mhartree (care must be used in the choice of the auxiliary basis set, especially for the larger systems).

A numerical integration is necessary for the evaluation of the exchange−correlation potential and energy. The scheme used in this work adopts well-known techniques that partition the density into atomic contributions;[32] this "atomic density" is then integrated using a radial quadrature and a highly efficient angular quadrature.[33] One hundred twenty-three points were used for the radial part. Five hundred ninety points were used for the angular part, corresponding to the exact integration of all spherical harmonics up to $\ell = 41$. For the radial quadrature, the scheme of ref 34 has been rescaled[35] in order to better integrate the contribution coming from the diffuse functions present in the basis set. Such an extensive grid is necessary to keep numerical accuracy under control in these complicated systems, with s, p, and d mutually interacting open shells. Tests have shown that using lower quality numerical grids or charge density auxiliary basis sets may lead to even qualitatively incorrect results or slow convergence.

As in ref 14, the geometry optimization was stopped when maximum force on atoms was less than 4×10^{-4} au.

The exploitation of symmetry is obviously beneficial to reduce the computational effort. For example, the CPU time ratios among the different symmetries for Pt_{13} using basis set A on a single processor of a Compaq Alpha XP-1000 667 MHz computer are

O_h	D_{4h}	I_h	D_{5h}	C_{2h}	C_{2v}	C_1
1	1.7	2.2	2.7	4.6	4.8	16.9

It is to be noted that CPU time $I_h > D_{4h}$, O_h even though I_h is a higher group. This is due to the fact that the Lebedev angular grid[33] exhibits cubic symmetry, so that symmetry is not fully exploited when C_5 axes are present (the precise figure will in general depend on the ratio between the computational effort involved in the evaluation of the Coulomb potential and the numerical integration).

NWChem is a suite of programs specifically developed for parallel computers, and is based on a distributed memory approach for parallelism.[23] The use of an auxiliary charge density basis set can be particularly advantageous in this respect, because one expects super-linear scaling whenever the aggregate memory is sufficient to store all the three-center integrals in the memory available on the parallel hardware (which are therefore not recalculated at each iteration step). To give an idea of the computational effort involved in the calculations, we quote that a single SCF cycle for O_h Pt_{55} using the present

TABLE 1: The Results of DF Calculations Using Basis Set A on Pt_{13}^q ($q = 0, \pm 1$) in Various Structural Arrangements (Described in the Text) Are Reported[a]

system	ΔE	$N_\alpha - N_\beta$	BW (α/β)	gap (α/β)	ϵ_F	geometry
I_h	1.086	2	7.30/7.43	0.13/0.13 h_g^3	−5.242	2.671
I_h	1.065	8	7.57/7.49	0.82/0.03	−5.101	2.687
T_h	1.003	8	7.49/7.45	0.80/0.06 t_g^1	−5.098	2.684, 2.744, 2.842
O_h	0.720	6	6.96/7.04	0.86/0.19 $t_{2u}-e_g$ 0.001	−5.264	2.723
D_{5h}	0.230	4	7.12/7.17	0.36/0.18 e_{2g}^1	−5.082	2.906, 2.677 (0.463)
C_{2v}	0.186	4	7.12/7.09	0.30/0.15	−5.071	2.907, 2.63−2.72(0.465)
D_{4h}	3.297	2	7.48/7.36	0.11/0.31	−5.137	3.179, 2.526 (0.908)
I_h^+	1.295	3	7.39/7.43	0.10/0.10 h_g^2	−8.902	2.672
T_h^+	1.057	9	7.49/7.42	1.01/0.07	−8.786	2.684, 2.744, 2.842
O_h^+	0.902	7	6.85/7.05	1.1/0.17 $t_{2u}-e_g$ 0.008	−8.859	2.725
D_{5h}^+	0.264	5	7.15/7.15	0.35/0.06	−8.745	2.946, 2.672 (0.460)
D_{4h}^+	6.858	1	7.47/7.34	0.09/0.28	−8.652	3.158, 2.534 (0.902)
I_h^-	0.965	1	7.30/7.32	0.17/0.17 h_g^4	−1.674	2.810
C_{2h}^-	0.909	1	7.33/7.34	0.15/0.10	−1.609	2.63−2.70, 2.76−2.82, 2.80−2.83
O_h^-	0.566	5	6.91/6.97	0.70/0.22	−1.732	2.725
D_{5h}^-	0.250	3	7.07/7.10	0.36/0.18	−1.411	2.874, 2.685 (0.465)
D_{4h}^-	3.342	3	7.37/7.18	0.06/0.26	−1.585	3.145, 2.548 (0.898)

[a] $N_\alpha - N_\beta$ is the difference in the number of α and β electrons; BW and gap are the band width and the HOMO−LUMO energy difference for α/β electrons, respectively; ϵ_F is the Fermi energy; and geometry lists representative atom−atom distances as explained in the text. In the case of JT or pJT systems, HOMO symmetry labels are explicitly reported on the right of the gap value, together with their energy difference. The ΔE column has a mixed meaning, reporting the binding energy per atom BE/N in the case of the lowest energy minimum (D_{4h} for Pt_{13}), the electron affinity and ionization potential for the lowest energy ionic structures (D_{4h}^- and D_{4h}^+, respectively, for Pt_{13}), and the excitation energy with respect to the lowest energy configuration of each charge state for all other configurations. Energy-related quantities are in eV, distances in angstroms.

methodology requires ∼2300 s when running on a Compaq Alpha XP-1000 667 MHz computer.

To overcome the degeneracy problems that arise in systems such as these, containing many transition metals in low oxidation state, a Gaussian-smearing technique for the fractional occupation of the energy levels was applied.[36,37] This was not used to mimic Fermi−Dirac statistics at finite temperatures, nor was a many-determinantal wave function used to take into account long-range correlation effects.[38] However, smearing the one-electron levels is very beneficial if not strictly necessary to obtain a smooth convergence for such quasi-metallic systems, with very many levels extremely close in energy. The NWChem program has been purposely modified, and this new feature is available in the NWChem 4.1 release. Usually, the use of an error function with a broadening factor $\sigma = 0.006$ au is sufficient for obtaining a good convergence at the beginning of the SCF process, while $\sigma = 0.0003$ au was used for final convergence. All the results reported below have thus been obtained using $\sigma = 0.0003$ au and ∼0.01 eV.

If at convergence the HOMO−LUMO gap is appreciably larger than σ, then the use of smearing does not affect the final energy value (it is simply a tool to improve convergence). However, when restraining the system to have a definite (high) symmetry, one can find either an incomplete occupancy of a degenerate HOMO: Jahn−Teller systems (JT) or an accidental quasi-degeneracy between HOMO and LUMO in one spin symmetry: pseudo-Jahn−Teller systems (pJT). In such cases, the use of smearing makes a difference. For JT systems, in particular, it ensures an even occupation of all degenerate HOMOs, allowing one to perform calculations within the given symmetry group (no symmetry breaking). To be specific, for example, for neutral Pt_{13} we found one JT system (D_{5h}) and two pJT systems (O_h and I_h). In the case of Pt_{13}, starting from the geometry optimized at high symmetry, we have evaluated the gradient with respect to atomic displacements with the use of symmetry turned off; this gradient has resulted to be of a lower symmetry, which has finally been imposed in a further geometry optimization. This should guarantee that the final structures are local minima on the energy hyper-surface. Note that, for JT systems, $\sigma = 0$ has to be set in order to break symmetry.

A noteworthy advantage of the electron-smearing technique is that the difference in the number of α and β electrons takes its optimal value since no constraint is imposed on the spin multiplicity.[36,37] To check that this holds in a specific example, in analogy with ref 10 we have calculated for O_h Pt_{13} ($N_\alpha - N_\beta = 6$, see Tables 1 and 2 below) the solutions obtained without using the electron-smearing technique, but imposing a different value of $N_\alpha - N_\beta$, and found that these solutions existed at a higher energy.

Apart from the electron smearing, the exploitation of symmetry is extremely important to obtain a smooth convergence of the iterative process: for example, level-shifting techniques (with $\sigma = 0$) had to be used when dealing with low-symmetry configurations, such as C_{2v} Pt_{13}, as we were unable to obtain convergence even using electron smearing with high values of σ.

Unrestricted spin calculations have always been performed. The value of $\langle S^2 \rangle$ has been taken as an indicator of spin-symmetry breaking:[39] it usually differed from the spin-restricted value by less than 1%, except for few cases which will be explicitly indicated in the following.

3. Results

The results of DF/BPW91 calculations will be reported in this section, divided according to the number of atoms in the cluster.

Pt_{13}. Our results are collected in Table 1 (basis set A) and Table 2 (basis set B). For reasons of synthesis, the ΔE column in these and the following Tables has a mixed meaning, reporting the binding energy BE per atom BE/N in the case of the lowest energy minimum (D_{4h} for Pt_{13}), the electron affinity and ionization potential for the lowest energy ionic structures (D_{4h}^- and D_{4h}^+, respectively, for Pt_{13}), and the excitation energy with respect to the lowest energy configuration of each charge state for all other configurations.

The bandwidth BW reported in the tables is defined as the difference between the one-electron energies of the lowest and

TABLE 2: The Results of DF Calculations Using Basis Set B on Pt_{13}^q ($q = 0, \pm 1$) in Various Structural Arrangements (Described in the Text) Are Reported[a]

system	ΔE	$N_\alpha - N_\beta$	BW (α/β)	gap (α/β)	ϵ_F	E_{relax}	geometry
I_h	1.233	2	7.45/7.49	0.13/0.12 $\underline{h_g}^3$	−5.211	0.71	2.671
I_h	1.201	8	7.70/7.60	0.83/0.03	−5.081	0.74	2.686
O_h	0.701	6	7.00/7.09	0.90/0.21 $t_{2u}-e_g$ 0.009	−5.300	0.24	2.725
D_{4h}'	0.250	8	7.20/7.02	0.40/0.13	−5.081	1.86	3.147, 2.583 (0.965)
D_{5h}	0.221	4	7.20/7.27	0.36/0.16 $\underline{e}_{2g}^1$	−5.086	0.76	2.914, 2.678 (0.462)
D_{4h}	3.228	2	7.61/7.47	0.08/0.29	−5.189	2.11	3.181, 2.528 (0.905)
I_h^+	1.206	9	7.61/7.61	1.10/0.02 $\underline{h_g}^2$	−8.791		2.682
O_h^+	0.895	7	6.92/7.12	1.13/0.19 $t_{2u}-e_g$ 0.0006	−8.933		2.727
D_{5h}^+	0.248	5	7.26/7.26	0.36/0.07	−8.819		2.950, 2.673 (0.460)
D_{4h}^+	6.907	1	7.59/7.47	0.07/0.25	−8.724		3.166, 2.536 (0.903)
I_h^-	1.215	1	7.40/7.42	0.17/0.15 $\underline{h_g}^4$	−1.555		2.672
O_h^-	0.561	5	7.01/7.04	0.69/0.23 $t_{1g}-e_g$ 0.016	−1.713		2.726
D_{5h}^-	0.309	3	7.15/7.20	0.36/0.15	−1.357		2.881, 2.685 (0.464)
D_{4h}^-	3.359	3	7.38/7.26	0.06/0.26	−1.572		3.145, 2.550 (0.892)

[a] Notations are the same as those In Table 1, except for E_{relax}, which is the energy difference in eV between the "idealized" and optimized geometries. Energy-related quantities are in eV, distances in angstroms.

the highest occupied molecular orbitals. The gap value is defined as the difference between the one-electron energies of the HOMO and LUMO: a small value will be taken as an indication of the metallic character of the clusters. In the case of JT or pJT systems, all the (quasi-)degenerate orbitals have been considered as HOMOs, correspondingly taking average values of the various quantities. In these cases, the HOMO symmetry labels and energy differences are reported on the right of the gap values.

To avoid excessive duplications, not all states and quantities are reported in the two tables: in Table 2 only the basic states are reported, to be compared with the results for Pt_{38} and Pt_{55} using the same basis set. All the geometries have been fully optimized within the given symmetry group starting from "idealized" geometries, i.e., in which the basic Pt−Pt distance was set to $R_0 = 2.774$ Å (bulk crystal[40]). For O_h geometries, which correspond to a section of the face-centered cubic (fcc) crystal, this completely defines the atomic arrangement. Two distances characterize the I_h and D_{5h} geometries: the shorter one corresponds to the inter-shell distance for I_h and most of the distances for D_{5h}; the longer one to the intra-shell distance for I_h and a few distances for D_{5h}. The ratio between the two is

$$\sqrt{2(1 - 1/\sqrt{5})} \sim 1.05146$$

We set the shorter distance in idealized structures to 2.774 Å, which implies that the strained distance is equal to ∼2.915 Å. The relaxation energies E_{relax} reported in Tables 2, 4, and 5 refer to this choice of idealized geometries (for Pt_{13} the relaxation energy is only reported for basis set B).

As anticipated in section 2, for Pt_{13} the octahedral, icosahedral, and truncated decahedral geometries have been relaxed in the absence of symmetry until a local energy minimum was found. Let us start by looking at which kind of symmetry breaking one finds in each case.

Neutral D_{5h} Pt_{13} is a JT system, having a degenerate incompletely occupied e_{2g}^1 HOMO in the minority β spin symmetry. The structure deforms to a C_{2v} geometry. The energy gain is however small: only 0.044 eV. Adding or removing an electron from the e_{2g} orbital produces a system with a finite gap.

Neutral I_h Pt_{13} is a more complicated case, and very difficult to converge, because of an accidental quasi-degeneracy between a t_{2g} and a $\underline{h}_g$ orbitals close to the Fermi energy (here and in the following, β spin−orbitals will be denoted by underlining: $\underline{h}_g$), which implies a quasi-degeneracy between two electronic configurations:

high spin:	$h_g^5 t_{2g}^3 \underline{h}_g^0$	$N_\alpha - N_\beta = 8$
low spin:	$h_g^5 t_{2g}^0 \underline{h}_g^3$	$N_\alpha - N_\beta = 2$

differing in energy by ∼0.02−0.03 eV (see Tables 1 and 2). Of course, any change in the functional, but even in the basis set or the numerical procedure can reverse the order between the high- and low-spin states. By allowing symmetry breaking, the I_h configuration relaxes to a T_h or a C_{2h} one, depending on the charge state, but the energy lowering is again modest: 0.06 eV, except in the cation I_h (I_h^+) case, where however we were not able to converge to the high-spin state. An unusually high value of $\langle S^2 \rangle$ for C_{2h}^- Pt_{13}: $\langle S^2 \rangle = 1.152$ with $N_\alpha - N_\beta = 1$, testifies this quasi-degeneracy (the value of $\langle S^2 \rangle$ differs significantly from the spin-restricted one also for D_{4h}^- Pt_{13}: $\langle S^2 \rangle = 8.767$ with $N_\alpha - N_\beta = 3$).

Symmetry breaking is only important for the octahedral geometry, in which case one finds that a $O_h \rightarrow D_{4h}$ distortion lowers the energy by a substantial amount: 0.7, 0.9, and 0.5 eV for Pt_{13}^q with $q = 0, +1, -1$, respectively. The D_{4h} distorted geometry thus turns out to be the lowest energy one, surpassing the D_{5h} (C_{2v}) one by ≥0.2 eV at any charge state. In Table 2, therefore, only the D_{4h}, D_{5h}, O_h, and I_h states have been considered.

Before further relaxation, the order of the structure is: $D_{5h} < O_h < I_h$, irrespective of the charge state. This is at variance with the expectations of more simplified approaches[2,3,7] (atom−atom potentials, counting of the number of first neighbors, etc.) according to which the order should be $I_h < D_{5h} < O_h$: see below for a discussion. It is to be noted that low-spin states prevail, especially for the lowest energy configurations, in agreement with the fact that platinum is a nonmagnetic metal. The values of bandwidth BW and Fermi energy ϵ_F are similar for the different configurations, with the BW in the following order: $O_h < D_{5h} < D_{4h} \sim I_h$. Noteworthy is the variation of ϵ_F with the charge state.

By comparing the results with different charge, one finds that the addition or removal of an electron does not seem to affect much these clusters. All the characteristic quantities stay practically unchanged, apart from a "rigid-band" shift of all one-electron levels. In fact, we have checked that for each geometry even the electronic configuration stays the same, apart obviously from the orbitals directly involved in the charging process. Also the excitation energies of the various structural arrangements

do not change much: the order is $D_{4h} < D_{5h} < O_h < I_h$ for all cases, with D_{5h} at higher energy by 0.2−0.3 eV with respect to the D_{4h} ground state, O_h by ∼0.6−0.9 eV and I_h by ∼1.0−1.2 eV. The values of the geometrical parameters exhibit slightly larger differences, especially for I_h and D_{5h}.

By comparing the results of Tables 1 and 2, one sees that the smaller basis set (B) reproduces very well the results of the larger one (A). Apart from the binding energy BE per atom BE/*N*, which is larger for D_{4h} Pt_{13} by 0.07 eV when using basis set A, all the other energy differences, bandwidths, gaps, Fermi energies, and optimized geometrical parameters are accurately reproduced. We have also checked that the electronic configurations are the same using the two basis sets. Only the basis set B will thus be utilized for the calculations on the larger clusters: Pt_{38} and Pt_{55}.

Let us now discuss the structural results. The I_h and O_h structures have only one degree of freedom, which is the one reported in Tables 1 and 2: the distance between the central and the peripheral atoms. In the O_h structure, all the distances are the same. In the I_h structure, the distances among peripheral atoms are larger by a factor ∼1.051. The I_h structure can relax to a T_h or C_{2h} geometry. In the former (T_h) case, all peripheral atoms stay on a sphere, but six pairs of bonds in each of the plus/minus Cartesian directions shrink with respect to the other 30 surface bonds: these three distances are reported in Table 1. Note that T_h Pt_{13} is still a JT system, with a t_g^1 electronic configuration at the Fermi level. However, further symmetry breaking to C_{2h} geometry has a negligible effect on the energy, and has not been reported in Table 1. In the latter (C_{2h}) case, the original 12, 6, and 30 nearest-neighbor bonds of the T_h structure spread in such a way that it is difficult to describe. In Table 1 the range in which these bonds spread is reported.

The D_{5h} structure has three degrees of freedom which are reported in Tables 1 and 2: the distance of the two apical and of the 10 off-C_5 peripheral atoms from the central one, and the ratio between the absolute values of the *z*-coordinate of the off-C_5 atoms and the apical atoms (*z* is the C_5 axis). This ratio should be 0.5 in an idealized structure; its being smaller suggests that the (100) faces are larger than their optimal size, as expected on the basis of a Wulff construction reasoning.[2,3,7] When D_{5h} Pt_{13} relaxes to a C_{2v} structure, the two regular pentagons on which the ten C_5 atoms are distributed deform to two irregular ones. Again, the range in which the distances from the central atom spread is reported.

The most interesting case is the $O_h \rightarrow D_{4h}$ deformation. The O_h idealized cuboctahedron section of the fcc lattice is shown in Figure 1. The two (100) planes (or faces) along the *z*-axis are at a distance $(2)^{1/2}R_0 = 3.92$ Å, and are separated by a "crown" of four atoms in the $\pm x$ and $\pm y$ directions, at a distance $R_0 = 2.774$ Å from the central atom. For neutral Pt_{13} this structure is at 0.94 eV from the D_{4h} lowest energy state, and lowers to 0.72 eV after relaxation of the nearest-neighbor distance to 2.725 Å (results using basis set B from Table 2). The D_{4h} lowest energy configuration is also shown in Figure 1: with respect to the O_h structure, the (100) planes in the $\pm z$ directions get closer to each other (from 3.92 to 3.12 Å) and slightly enlarge (the nearest-neighbor distance increases from 2.774 to 2.82 Å), while the four "crown" atoms get further from the central one (from 2.774 to 3.17 Å). This structure may resemble an idealized body-centered cubic (bcc) structure (also shown in Figure 1), section of eight first and four second neighbors around the central atom of an hypothetical bcc crystal with nearest-neighbor distance set equal to 2.774 Å. However, in the bcc-like structure, the edges of the (100) faces are larger: 3.20 Å, so that the distance between atoms on the cube is the same as the second-neighbor distance (3.20 Å), and the bcc-idealized structure is at 2.11 eV over the D_{4h} ground state. The D_{4h} lowest energy structure therefore represents something between the bcc and fcc geometries, which differs substantially from both of them. This is confirmed by the fact that if one starts the geometry optimization from the bcc structure, one finds a different D_{4h} local minimum (denoted D_{4h}' in Table 2) in which the edge of the (100) faces is 2.95 Å; these faces are at a distance of 3.05 Å, and the peripheral atoms are at 3.15 Å from the central one (high spin: $N_\alpha - N_\beta = 8$). This structure resembles more the bcc idealized one, but is at 0.25 eV above the D_{4h} lowest energy configuration. The presence of low-lying local minima corresponding to structural isomers (even exhibiting the same symmetry) can have an influence on the mechanical properties of Pt nanoclusters. The peculiarity of the D_{4h} structure is also confirmed by the calculations reported in Table 3, where binding energies are reported for the sequence: Pt_9, Pt_{11}, Pt_{13}, and Pt_{15}, i.e., starting with a central atom surrounded by a cube of eight first-neighbors (Pt_9) and by progressively adding pairs of second neighbors on opposite faces of the cube. The BE increases by 8.34 eV from O_h Pt_9 to D_{4h} Pt_{11}, and by 8.63 eV from D_{4h} Pt_{11} to D_{4h} Pt_{13}, but only by 8.25 eV from D_{4h} Pt_{13} to D_{2h} Pt_{15}, which is moreover a pJT system, and, as such, is not particularly stable.

TABLE 3: Binding Energies BE in eV for the Sequence Pt_{9n}−Pt_{15}, from DF/BPW91 Calculations Using Basis Set A

system	BE	$N_\alpha - N_\beta$	degener
O_h Pt_9	25.91	2	no
D_{4h} Pt_{11}	34.23	0	no
O_h Pt_{13}	42.14	6	yes
D_{4h} Pt_{13}	42.86	2	no
O_h Pt_{15}	51.07	6	yes
D_{2h} Pt_{15}	51.11	6	yes

[a] The keyword "degener" indicates whether the systems are pJT ones (degener = yes) or have a finite gap at the Fermi level (degener = no). $N_\alpha - N_\beta$ Is the difference in the number of α and β electrons.

It is interesting to note that the relaxation energy, i.e., the difference between the idealized geometry and the optimized one, is minimal for the fcc (O_h) structure: ∼0.2 eV, intermediate for the C_5-axis structures, D_{5h} and I_h, ∼0.7 eV, and largest for the D_{4h} one, ∼2.1 eV. Even though the definition of idealized I_h and D_{5h} structures is not unique, these are the expected trends,[2] again with the only exception of the D_{4h} state.

The results for I_h and O_h Pt_{13} are comparable with those reported in the most recent work on these systems[10] (whose analysis of the orbital shell structure we refer to), after allowing for the differences due to the density functional, basis set, pseudopotential, and numerical approach. The main difference with respect to ref 10 is that the authors did not consider the D_{5h} structure and that a limited account of the Jahn−Teller distortion for the O_h structure hindered them from finding the D_{4h} ground state. In passing, it can be noted that the $I_h - O_h$ energy difference comes out to be much smaller from the calculations of ref 11, confirming the limitations of the Harris functional as applied to transition metal clusters.[9]

Pt_{38}. The results of DF calculations on Pt_{38}^q truncated octahedral cluster ($q = 0, \pm 1$) using basis set B are reported in Table 4. With respect to Pt_{13} one can observe a general increase in the BW, BE, and electron affinity values, and a decrease in the gap and ionization potential values, as expected. It is also to be noted the spin quenching effect, which now gives a closed-shell Pt_{38} neutral cluster. The value of $\langle S^2 \rangle$ differs significantly from the spin-restricted one only for O_h^+ Pt_{38}: $\langle S^2 \rangle = 1.001$ with $N_\alpha - N_\beta = 1$.

TABLE 4: The Results of DF Calculations on Truncated Octahedral Pt_{38}^q ($q = 0, \pm 1$) Are Reported[a]

system	ΔE	$N_\alpha - N_\beta$	BW (α/β)	gap (α/β)	ϵ_F	E_{relax}	geometry
O_h	3.876	0	8.19	0.07	−5.431	1.58	1.911, 4.311 (0.504), 3.631
O_h^+	6.760	1	8.20/8.21	0.09/0.08 $a_{1g}-t_{2u}^2$ 0.002	−8.059	-	1.914, 4.311 (0.504), 3.629
O_h^-(neu)	4.148	1	8.22/8.19	0.06 t_{1u}^1/0.06	−2.982	-	see fcc
O_h^-	4.202	7	8.24/8.14	0.02 t_{1g}^1/0.12	−2.998	-	1.908, 4.298 (0.501), 3.681
fcc							1.961, 4.386 (0.500), 3.397

[a] Notations are the same as those in Tables 1 and 2: in particular, the ΔE column reports the binding energy per atom BE/*N* in the case of the lowest energy neutral minimum, and the electron affinity and ionization potential for the lowest energy ionic structures. O_h^-(neu) stands for the result of a calculation on the Pt_{38}^- anion taken at the geometry of neutral O_h Pt_{38}. fcc is the "ideal" geometry corresponding to a section of the fcc crystal. Energy-related quantities are in eV, distances in angstroms.

TABLE 5: The results of DF Calculations On Cuboctahedral (O_h), Truncated Decahedral (D_{5h}), and Icosahedral (I_h) Pt_{55}^q ($q = 0, \pm 1$) Are Reported[a]

system	ΔE	$N_\alpha - N_\beta$	BW (α/β)	gap (α/β)	ϵ_F	E_{relax}	geometry
O_h	0.471	10	8.65/8.65	0.17/0.06	−5.379	1.703	2.734, 4.168, 4.792 (1.033), 5.420
D_{5h}	0.240	8	8.81/8.74	0.04 e^1_u/0.11	−5.364	2.183	2.72−2.79, 4.04, 4.71−4.86, 5.37−5.62
I_h	3.994	12	9.13/9.32	0.28/0.04	−5.511	3.807	2.651, 4.686, 5.233
O_h^+	0.364	11	8.61/8.63	0.20/0.04	−7.705		2.733, 4.201, 4.785 (1.032), 5.423
D_{5h}^+	0.010	7	8.78/8.76	0.05/0.09	−7.665		2.72−2.79, 4.04, 4.70−4.85, 5.37−5.61
I_h^+	6.545	13	9.13/9.31	0.29/0.03	−7.849		2.650, 4.686, 5.233
O_h^-	0.137	9	8.63/8.69	0.18/0.08 $e_u^{0.6}t_{2u}^{0.4}$	−3.082		2.735, 4.167, 4.792 (1.033), 5.421
D_{5h}^-	0.130	9	8.78/8.74	0.04/0.11	−3.081		2.72−2.80, 4.04, 4.72−4.86, 5.37−5.61
I_h^-	4.216	11	9.14/9.31	0.20/0.08 $t_{2g}^{2.2}g_g^{2.1}g_u^{0.7}$	−3.216		2.651, 4.686, 5.234

[a] Notations are the same as those In Tables 1 and 2: in particular, the ΔE column reports the binding energy per atom BE/N in the case of the lowest energy minimum (I_h for Pt_{55}), the electron affinity and ionization potential for the lowest energy Ionic structures (I_h^- and I_h^+, respectively, for Pt_{55}), and the excitation energy with respect to the lowest energy configuration of each charge state for all other configurations. Energy-related quantities are in eV, distances in angstroms.

We have checked also for Pt_{38} that the electronic configuration stays the same after the charging process, apart of course from the orbital directly involved. An exception is Pt_{38}^-. In this case, in fact, the electronic configuration of the anion changes in passing from the geometry optimized for the neutral molecule, $t_{1u}^1t_{1g}^0t_{2u}^3$, $N_\alpha - N_\beta = 1$, to that optimized for the anion itself, $t_{1u}^3t_{1g}^1t_{2u}^0$, $N_\alpha - N_\beta = 7$. This happens because the involved orbitals and corresponding configurations are all very close to the Fermi level, and a tiny structural rearrangement is sufficient to exchange their order: see Table 4. Apart from this, however, one finds that the charging process does not influence much the electronic and structural properties of O_h Pt_{38}, from a quantitative point of view even less than for Pt_{13}, as expected.

A very interesting result is the structural one. Pt_{38}, in fact, as a truncated octahedron should be a nearly optimal example of crystalline geometry, as the ratio between (100) and (111) faces is much more favorable than in the case of the cuboctahedral arrangement.[2,3,7] This is the reason Pt_{38} has been included in our analysis, even though we cannot compare it with other configurations of different symmetry containing the same number of atoms. One has three nonequivalent atoms for O_h Pt_{38}. In the first shell, one finds six atoms in an octahedral arrangement; in the second shell, one finds 24 atoms lying at the vertexes of the six (100) faces and eight atoms lying at the center of (111) faces (see Figure 1 for a schematic picture of the cluster). Correspondingly, one has four degrees of freedom: the distances of the three nonequivalent atoms from the center of the cluster, and the ratio of the minor over the major Cartesian components of the 24 (100) atoms (this ratio should be 0.5 for an idealized structure). From Table 2, one sees that this ratio has a value very close to the ideal one: this confirms that the (100) faces are only slightly larger than their optimal size.[7] However, the three nonequivalent atoms exhibit a very different (inhomogeneous) radial relaxation: the atoms in the first shell or on the (100) faces relax inward by 1.8−2.7%, whereas the atoms on the (111) faces relax outward by 6.8−8.4%. This peculiar structural rearrangement resembles that found for O_h Pt_{55} in ref 14 (and confirmed by the present calculations, see below), and seems to be a general feature of platinum nanoclusters, a feature not predicted by more simplified methods such as atom−atom potentials,[7] in which all the surface atoms tend to relax inward, the more the less bound they are. Such a behavior is probably connected with the tendency of Pt surfaces to peculiar reconstructions.[41−44]

Pt_{55}. The results of DF calculations on I_h, D_{5h}, and O_h Pt_{55}^q clusters ($q = 0, \pm 1$) using basis set B are reported in Table 5. The structures of these clusters can be obtained from those of the corresponding Pt_{13} clusters depicted in Figure 1 by adding another shell of atoms around the Pt_{13} "core". Their appearance is thus similar to the structures shown in Figure 1, with the only difference that all the edges contain three atoms instead of two, and there is a further atom at the center of the (100) faces. From an analysis of Table 5, several points are worth mentioning.

First, the order of the structures has changed with respect to Pt_{13} and is now $I_h < D_{5h} < O_h$. The energy differences are much smaller than for Pt_{13}. Furthermore, the lowest energy configuration is now the icosahedral one, in contrast with the expectations of more simplified approaches.[2,3,7] It is known in fact that icosahedral clusters have more favorable surface energies with respect to crystalline structures, but also larger strain for the interior atoms, due to the mismatch between intra- and intershell distances imposed by symmetry constraints. From general bonding considerations,[2,3,7] one thus expects icosahedral configurations to become less and less favored with increasing size. The fact that we found an opposite behavior implies that in our first-principles approach Pt_{13} presents peculiar characteristics of a finite system (e.g., occupation of unfavoured one-electron orbitals due to symmetry reasons) that are difficult to insert in a smooth behavior of the structural properties as functions of the cluster size. In contrast, Pt_{55} seems to conform reasonably well to atom−atom predictions,[7] and to be located about the crossover among 5-fold and crystalline structures (see the small values of the energy differences). The final DF/BPW91 predic-

TABLE 6: Number of Formal Nearest-Neighbor Bonds *B* and Extrapolated Values (in eV) of BE/*N* for the Various Structures Considered in the Present Work

system	B	extrapolated BE/N
I_h Pt_{13}	42	5.9
D_{5h} Pt_{13}	37	6.8
O_h Pt_{13}	36	6.9
O_h Pt_{38}	144	6.1
I_h Pt_{55}	234	5.6
D_{5h} Pt_{55}	219	6.0
O_h Pt_{55}	216	6.1

tion is thus that icosahedral arrangements are possible candidates (among the highly symmetrical ones) as the lowest energy structures for bare platinum nanoclusters with a number of atoms less than 100. This conclusion is attenuated by the fact that our comparison is taken at sizes which are optimal for the icosahedral structures, but not for the fcc or decahedral arrangements, which presents too large (100) faces at $N = 55$.[5] Better D_{5h} or O_h structures, with smaller (100) faces, can be obtained at other sizes through the Wulff construction,[2,3,7] which gives, for example, Pt_{38} for O_h or a particularly good D_{5h} candidate at $N = 75$.

Apart from the order of the structures, the other descriptors do not present surprises. The BW follows the same order as in Pt_{13}, i.e., $O_h < D_{5h} < I_h$, the gap values correspondently decrease, and charging the clusters does not produce qualitative modifications: we have checked also for Pt_{55} that the electronic configurations do not change with the charge state of the clusters (the only exception is I_h Pt_{55}, for which one finds a switch in the one-electron levels analogous to that for Pt_{38}^-).

The BE, electron affinities EA, and ionization potentials IP show the expected trend with respect to Pt_{13}.

The BE may be extrapolated to the bulk limit using the average coordination number ACN as in ref 14. One can calculate the ACN for the various clusters by counting the number of formal bonds, and then extrapolating to ACN = 12. The results of this extrapolation are given in Table 6. It can be noted that (a) despite the fact that BE(D_{5h} Pt_{13}) > BE(O_h Pt_{13}), the extrapolated value for the O_h structure is larger than that for the D_{5h} structure; (b) the extrapolated values for O_h Pt_{38} and O_h Pt_{55} coincide, despite the fact that Pt_{38} is a smaller cluster: this confirms that Pt_{55} is not a particularly stable fcc cluster.

It is useful to analyze the IP and EA values in terms of the spherical droplet model (SDM).[45] In this model, the intrinsic work function W_∞ of the metal is corrected for a cluster by the work to be done against the electric field of the charge remaining on the cluster (assumed to be at the surface of the cluster assimilated to a sphere of radius R), so that the formulas for IP(R) and EA(R) read as

$$\mathrm{IP}(R) = W_\infty + (\alpha + n - 1)\frac{e^2}{R}$$

$$\mathrm{EA}(R) = W_\infty - (\beta + n - 1)\frac{e^2}{R}$$

with W_∞ the intrinsic work function, n the ±charge, and α and β undefined parameters. The constraint $\alpha + \beta = 1$ is generally accepted, whereas there is no agreement on the ideal values for α and β, even though the ratio α/β is expected be around 3−4. We took the effective cluster radii as in ref 8 by averaging over all radial distances of the outermost shell nuclei and by adding half the nearest-neighbor bulk distance. The results derived from Table 2, 4, and 5 for the lowest energy state of each cluster size are presented in Figure 2. From this figure, it is apparent that the SDM fits the results reasonably well. The extrapolated value of the work function: $W_\infty \sim 6$. eV falls within the scattered range of experimental values.[46−51] The fitted value of the α/β ratio is about 3, as expected, and the overall appearance of Figure 2 is typical of this kind of plots.[45]

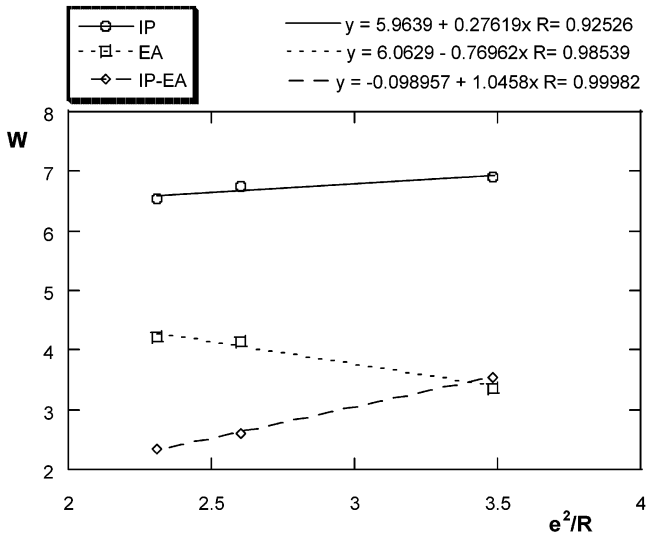

Figure 2. Ionization potential IP, electron affinity EA, and their difference (IP − EA) as functions of the inverse of the effective cluster radius R as defined in the text. In the equations, the results of a linear interpolation are shown, with y = fitted quantity (IP, EA, or IP − EA) in eV; $x = e^2/R$ in eV; and R = regression coefficient.

The structural results are again very interesting. For I_h Pt_{55} one has three nonequivalent atoms apart from the central one: 12 in the first shell, 12 at the vertexes, and 30 at the edges of the surface, whose distances from the central atoms are the degrees of freedom of the structure and are given in Table 5. For O_h Pt_{55}, one has four nonequivalent atoms apart from the central one: 12 in the first shell, 12 on the vertexes, 24 on the edges between (111) and (100) faces, and six at the center of the (100) faces of the surface. The degrees of freedom are the corresponding distances from the central atom, plus the ratio between the height of the (100) plane for the 24 edge atoms and the corresponding vertex atoms (the ideal value of this ratio is 1), and are given in Table 5. For D_{5h} Pt_{55}, one has eight nonequivalent atoms apart from the central one. In the first shell, we find two types of vertex atoms (10 + 2); in the second shell, two types of atoms at the vertexes (10 + 2), three types of atoms on the edges between (111) and (111), (111) and (100), and (100) and (100) faces, respectively, and one type of atom at the center of (100) faces of the surface. For the sake of simplicity, only the range of the distances from the central atom for first-shell atoms, and second-shell vertexes, edges, and faces is given in Table 5.

Two main points are worth noting,

(a) The geometries of the charged clusters are extremely similar to those of the neutral ones, with differences still smaller with respect to Pt_{38} and Pt_{13}, as expected.

(b) An *expansion* of the atoms at the center of (100) faces is found for O_h and D_{5h} Pt_{55}.

As for the latter point, to be specific for O_h Pt_{55}, the atoms in the first shell, the vertexes, and the edges of the surface shrink their distances from the center by 1.4%, 2.3%, and 0.3%, respectively, whereas the (100) atoms *expand* by 6.2%. Analogously, for D_{5h} Pt_{55} the angles *ABA* where B is a (100) atom and A is an atom at a vertex, or at an edge between (111) and (100) faces, or at an edge between two (100) faces, are 171.5°,

174.9°, and 169.5°, respectively. This kind of surface reconstruction is probably beneficial to release surface stress.[41−44] A similar but much smaller effect can be evinced for Pd_{55} from an inspection of Table 6 in ref 9.

We stress that the structural relaxation is strongly inhomogeneous,[6] with both a radial and a tangential pronounced character. It can be noted in particular the compression[6] of the inner shell in I_h Pt_{55} (from 2.686 to 2.651 Å), to be contrasted with the expansion in O_h Pt_{55} (from 2.725 to 2.734 Å), which is in agreement with the results of refs 6, 9, 52, and 53, using atom−atom or tight-binding approaches. This finding is in keeping with the well-known fact that the inner core of the crystalline structures progressively approach the bulk, whereas icosahedral structures remain something like a "giant molecule" at any size.[6,53] For D_{5h} Pt_{55}, one finds an intermediate situation: compression for the elongated v−c bonds, and expansion for the v′−c bonds, where v are the vertexes on the C_5 axis, v′ are the other vertexes, and c is the central atom.

4. Conclusions

We can summarize the conclusions of the present investigation in the following main points:

(a) Platinum clusters in this size range: Pt_n, $n = 13-55$, start developing metallic characteristics: we find a vanishing gap at the Fermi level, which produces in several cases quasi-degeneracies among different electronic configurations (see, for example, I_h Pt_{13} or O_h Pt_{38}^-). It is worth remarking that quasi-degeneracy between one-electron levels does not imply per se quasi-degeneracy between the corresponding electronic configurations, unless Coulomb interactions are effectively screened.

(b) The introduction of a ±charge produces small effects on Pt_{13} and even smaller on Pt_{38} and Pt_{55}; the optimized geometries are slightly affected, the order of the structures stays the same and the electronic configurations only change in the orbitals directly involved in the charging process, with the only exception of the quasi-degeneracy cases mentioned in point a.

(c) The energy order of the optimized symmetrical structure is $D_{5h} < O_h < I_h$ for Pt_{13} and $I_h < D_{5h} < O_h$ for Pt_{55}, even though the energy differences are smaller for Pt_{55} than for Pt_{13}. The anomalous behavior of Pt_{13} is interpreted as due to the small size of the molecule, while Pt_{55} seems to be intermediate between finite molecules and fully metallic systems.[54] In any case, the icosahedral structures seem to be possible competitors at these intermediate sizes, in agreement with the results of semiempirical potentials.[7] The presence of several structural isomers close in energy (see D_{4h}/D_{4h}' Pt_{13} above) may confer peculiar mechanical properties to these metallic clusters.

(d) For Pt_{13}, a D_{4h} configuration originating from the O_h one by symmetry breaking is predicted to be the lowest energy one. For Pt_{38} and Pt_{55}, a peculiar structural rearrangement is found, corresponding to an expansion (reconstruction) of the atoms lying on (111) or (100) faces. For Pt_{13} and Pt_{55}, the (100) faces tend to shrink whenever allowed by the symmetry constraints, whereas they seem to be at their optimal size for Pt_{38}.

(e) The spin is effectively quenched, especially for the most stable configurations, in agreement with the fact that platinum is a nonmagnetic metal.

(f) The binding energy per atom extrapolates reasonably well to the bulk value, and so do the ionization potential and electron affinity.

(g) A very accurate computational procedure is needed to keep numerical accuracy under control.

Acknowledgment. We gratefully acknowledge the Italian INSTM (Istituto Nazionale per la Scienza e Tecnologia dei Materiali) for a grant making available the resources of CINECA supercomputing center (Bologna, Italy) and Andrea Biagi (IPCF, Pisa, Italy) for technical assistance. A portion of the research described in this manuscript was performed at the W. R. Wiley Environmental Molecular Sciences Laboratory, a national scientific user facility sponsored by the U.S. Department of Energy's Office of Biological and Environmental Research and located at Pacific Northwest National Laboratory. Pacific Northwest National Laboratory is operated for the Department of Energy by Battelle.

References and Notes

(1) Klabunde, K. J. *Nanoscale Materials in Chemistry*; Wiley: New York, 2001.
(2) Marks, L. D. *Rep. Prog. Phys.* **1994**, *57*, 603.
(3) Martin, T. P. *Phys. Rep.* **1996**, *273*, 199.
(4) Cleveland, C. L.; Landman, U.; Schaaf, T. G.; Shafigullin, M. N.; Stephens, P. W.; Whetten, R. L. *Phys. Rev. Lett.* **1997**, *79*, 1873.
(5) Doye, J. P. K.; Wales, D. *J. New J. Chem.* **1998**, 733.
(6) Barretau, C.; Desjonquères, M. C.; Spanjaard, D. *Eur. Phys. J. D.* **2000**, *11*, 395.
(7) Baletto, F.; Ferrando, R.; Fortunelli, A.; Montalenti, F.; Mottet, C. *J. Chem. Phys.* **2002**, *116*, 3856.
(8) Haberlen, O. D.; Chung, J. C.;. Stener, M.; Rosch, N. *J. Chem. Phys.* **1997**, *106*, 5189.
(9) Jennison, D. R.; Schultz, P. A.; Sears, M. P. *J. Chem. Phys.* **1997**, *106*, 1856.
(10) Watari, N.; Ohnishi, S. *Phys. Rev. B* **1998**, *58*, 1665.
(11) Yang, S. H.; Drabold, D. A.; Adams, J. B.; Ordejòn, P.; Glassford, K. *J. Phys.: Condens. Matter* **1997**, *9*, L39.
(12) Yang, L.; DePriesto, A. E. *J. Chem. Phys.* **1994**, *100*, 725.
(13) Ahlrichs, R.; Elliot, S. *Phys. Chem. Chem. Phys.* **1999**, *1*, 13.
(14) Aprá, E.; Fortunelli, A. *J. Mol. Struct. (THEOCHEM)* **2000**, *501−502*, 251.
(15) Garzòn, I. L.; Posada-Amarillas, A. *Phys. Rev. B* **1996**, *54*, 11796.
(16) Häkkinen, H.; Moseler, M.; Landman, U. *Phys. Rev. Lett.* **2002**, *89*, 033401.
(17) Yeon-Wook, K.; Hong-Ming, L.; Kelly, T. F. *Acta Metall.* **1989**, *37*, 247.
(18) Martra, G.; Coluccia, S.; Monticelli, O.; Vitulli, G. *Catal. Lett.* **1994**, *29*, 105.
(19) . Contrata, W.; Mitchell M. J.; Mochel, J. M. *Ultramicroscopy* **1993**, *48*, 297.
(20) Rosato, V.; Guillopé M.; Legrand, B. *Philos. Mag. A* **1989**, *59*, 321.
(21) . Goringe, C. M.; Bowler, D. R.; Hernandez, E. *Rep. Prog. Phys.* **1997**, *60*, 1447.
(22) Fortunelli, A.; Velasco, A. M. *Int. J. Quantum Chem.* Submitted for publication.
(23) Harrison, R. J.; Nichols, J. A.; Straatsma, T. P.; Dupuis, M.; Bylaska, E. J.; Fann, G. I.; Windus, T. L.; Aprà, E.; Anchell, J.; Bernholdt, D.; Borowski, P.; Clark, T.; Clerc, D.; Dachsel, H.; de Jong, B.; Deegan, M.; Dyall, K.; Elwood, D.; Fruchtl, H.; Glendening, E.; Gutowski, M.; Hess, A.; Jaffe, J.; Johnson, B.; Ju, J.; Kendall, R.; Kobayashi, R.; Kutteh R.; Lin, Z.; Littlefield, R.; Long, X.; Meng, B.; Nieplocha, J.; Niu, S.; Rosing, M.; Sandrone, G.; Stave, M.; Taylor, H.; Thomas, G.; van Lenthe, J.; Wolinski, K.; Wong, A.; Zhang, Z. *NWChem, A Computational Chemistry Package for Parallel Computers*, version 4.1; Pacific Northwest National Laboratory, Richland, WA 99352-0999, 2002.
(24) Andrae, D.; Haeussermann, U.; Dolg, M.; Stoll, H.; Preuss, H. *Theor. Chim. Acta* **1990**, *77*, 123.
(25) Schaefer, A.; Huber, C.; Ahlrichs, R. *J. Chem. Phys.* **1994**, *100*, 5289.
(26) Becke, A. D. *Phys. Rev. A* **1988**, *38*, 3098.
(27) Perdew, J. P.; Wang, Y. *Phys. Rev. B* **1986**, *33*, 8800. Perdew, J. P.; Chevary, J. A.; Vosko, S. H.; Jackson, K. A.; Pederson, M. R.; Singh D. J.; Fiolhais, C. *Phys. Rev. B* **1992**, *46*, 6671.
(28) Fortunelli, A. *J. Mol. Struct. (THEOCHEM)* **1999**, *487*, 251.
(29) Dunlap, B. I.; Connolly J. W. D.; Sabin, J. R. *J. Chem. Phys.* **1979**, *71*, 4993.
(30) Fortunelli, A.; Salvetti, O. *J. Comput. Chem.* **1991**, *12*, 36.
(31) Eichkorn, K.; Treutler, O.; Öhm, H.; Häser M.; Ahlrichs, R. *Chem. Phys. Lett* **1995**, *242*, 652.
(32) Becke, A. D. *J. Chem. Phys.* **1988**, *88*, 2547.
(33) Lebedev, V. I.; Laikov, D. N. *Dokl. Math.* **1999**, *366*, 741. Delley, B. J. *Comput. Chem.* **1996**, *17*, 1152.
(34) Mura, M. E.and Knowles, P. J. *J. Chem. Phys.* **1996**, *104*, 9848. Murray, C. W.; Handy, N. C.; Laming, G. L. *Mol. Phys.* **1993**, *78*, 997.

(35) Aprà, E. Unpublished results. This rescaled grid is available in the 4.1 release of NWChem.
(36) Elsässer, C.; Fähnle, M.; Chan, C. T.; Ho, K. M. *Phys. Rev. B* **1994**, *49*, 13975.
(37) Warren, R. W.; Dunlap, B. I. *Chem. Phys. Lett.* **1996**, *262*, 384.
(38) Wang, S. G.; Schwartz, W. H. E. *J. Chem. Phys.* **1996**, *105*, 4641.
(39) Adamo, C.; Barone V.; Fortunelli, A. *J. Chem. Phys.* **1995**, *98*, 8648.
(40) Kittel, C. *Introduction to Solid State Physics*; Wiley: New York, 1968.
(41) Feibelman, P. J.; Nelson, J. S.; Kellogg, G. L. *Phys. Rev. B* **1994**, *49*, 10548. Feibelman, P. J. *Phys. Rev. B* **1995**, *51*, 17867.
(42) Oppo, S.; Fiorentini, V. *Phys. Rev. Lett.* **1998**, *81*, 4278.
(43) Filippetti, A.; Fiorentini, V. *Surf. Sci.* **1997**, *377*−*379*, 112; *Phys. Rev. B* **1999**, *60*, 14366.
(44) Fiorentini, V.; Methfessel, M.;. Scheffler, M. *Phys. Rev. Lett.* **1993**, *71*, 1051 and **1998**, *81*, 2184.
(45) Wood, D. M. *Phys. Rev. Lett.* **1981**, *46*, 749.
(46) Kiskinova, M.; Pirug, G.; Bonzel, H. P. *Surf. Sci.* **1983**, *133*, 321.
(47) Salmerón, R.; Ferrer, S.; Jazzar, M.; Somorjai, G. A. *Phys. Rev. B* **1983**, *28*, 6758.
(48) Derry, G. N.; Zhang, J.-Z. *Phys. Rev. B* **1989**, *39*, 1940.
(49) Alnot, M.; Ehrhardt, I. J.; Barnard, J. A. *Surf. Sci.* **1989**, *208*, 285.
(50) Cassuto, A.; Mane, M.; Hugenschmidt, M.; Dolle P.; Jupille, J. *Surf. Sci.* **1990**, *237*, 63.
(51) Kaack, M.; Fick, D. *Surf. Sci.* **1995**, *342*, 111.
(52) D'Agostino, G. *Mater. Sci. Forum* **1995**, *195*, 149.
(53) Fortunelli, A.; Velasco, A. M. *J. Mol. Struct. (THEOCHEM)* **2000**, *528*, 1.
(54) Fortunelli, A.; Velasco, A. M. *J. Mol. Struct. (THEOCHEM)* **1999**, *487*, 251.